INTER-FIBRE FAILURE UNDER COMPRESSION: BIAXIAL LODING

E. Correa*, F. París, V. Mantič

Group of Elasticity and Strength of Materials, Continuum Mechanics Dpt., School of Engineering, University of Seville, Camino de los Descubrimientos s/n, 41092 Seville (SPAIN)
**ecorrea@us.es*

Keywords: Inter-fibre failure; Micromechanics; BEM models; Biaxial loading.

Abstract

The influence of a secondary transverse load (tension or compression), perpendicular to the transverse compression nominally responsible for the failure, on the inter-fibre failure is studied at micromechanical level. The problem is analysed by means of the Boundary Element Method and under the light of Interfacial Fracture Mechanics. The results obtained show that the presence of a secondary tension accelerates the generation of failure whereas a secondary compression inhibits it.

1. Introduction

Many matrix/inter-fibre failure criteria assume that the failure occurring at a plane is governed by the components of the stress vector associated to that plane. In this work, an analysis of the influence of an out of failure plane stress component, i.e. secondary load (tension or compression), on the generation of the damage dominated by a transverse compression is carried out.

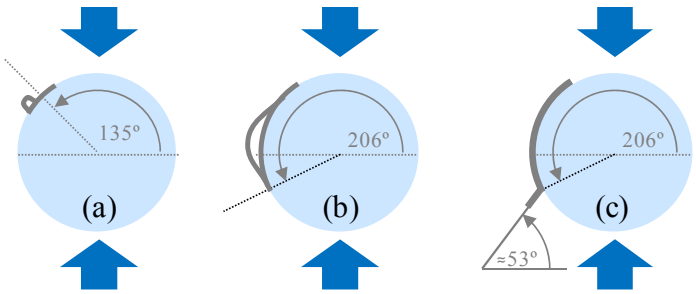

Figure 1. Initial stages of inter-fibre failure under uniaxial compression.

The inter-fibre failure under uniaxial compression starts with the appearance of small debonds at the fibre-matrix interfaces. In accordance with the previous studies of the authors [1,2] the initial defects present a non-symmetric morphology consisting in a small 'bubble' at the lower crack tip and a contact zone at the upper one, see Fig. 1(a). These initial cracks grow unstably along the interfaces from their lower crack tips. This stage ends when these cracks reach a certain length at the interface, which coincides with the closing of the 'bubble', Fig. 1(b). From that moment on the growth becomes stable and crack kinking towards the matrix is promoted (following an orientation angle, θ_{kink}, around 53º from the direction perpendicular to the load, Fig. 1(c)).

The study is performed by means of single-fibre BEM models and Interfacial Fracture Mechanics concepts [3] are employed for the analysis of the results.

2. Models

The numerical study has been performed using a tool based on BEM [4], able to consider contact between surfaces. Two single-fibre BEM models are used in this analysis. The size of the cell is large enough for the fibre to be considered as isolated. The basic model employed is shown in Fig. 2(a) and represents the case of a crack which, under the plane strain hypothesis, grows along the interface.

To characterize the problem from the Fracture Mechanics point of view, the Energy Release Rate (ERR), G, is used. The expression employed, based on [5], for a circular crack that propagates from a certain debonding angle, α, Fig. 2a, to $\alpha+\Delta\alpha$ ($\Delta\alpha << \alpha$), is:

$$G(\alpha,\Delta\alpha)=\frac{1}{2\Delta\alpha}\int_0^{\Delta\alpha}\left[\sigma_{rr}(\alpha+\theta)\Delta u_r(\alpha-\Delta\alpha+\theta)+\sigma_{r\theta}(\alpha+\theta)\Delta u_\theta(\alpha-\Delta\alpha+\theta)\right]d\theta \qquad (1)$$

where θ is the circumferential coordinate with reference to the 3-axis. σ_{rr} and $\sigma_{r\theta}$ represent, respectively, radial and shear stresses along the interface, and Δu_r and Δu_θ represent the relative displacements of the crack faces. Both modes of fracture, I and II are obviously considered in Eq. (1). For this study, $\Delta\alpha$ has been taken equal to 0.5º.

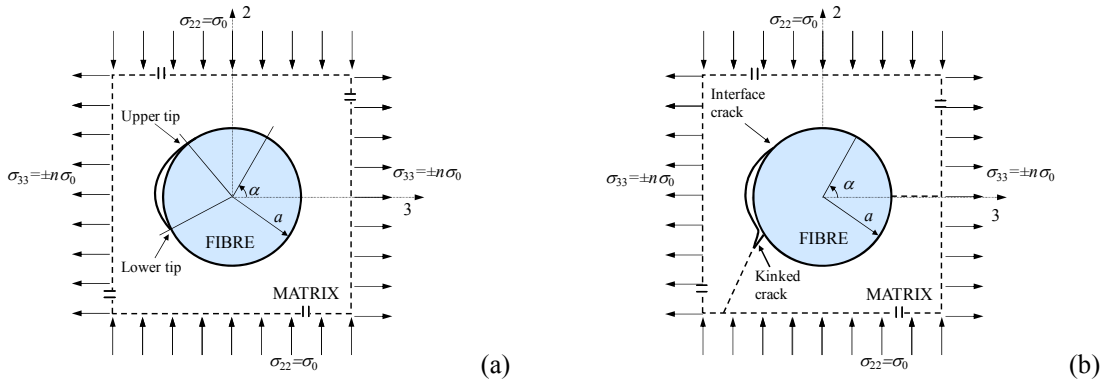

Figure. 2. Single fibre models: (a) interface crack, and (b) kinked crack in the matrix.

A second model, Fig. 2(b), is employed for the considering of a kinked crack in the matrix. The materials chosen for the analysis correspond to a glass fibre-epoxy matrix system whose elastic properties are: $E^m=2.79\times10^9$ Pa, $\nu^m=0.33$, $E^f=7.08\times10^{10}$ Pa and $\nu^f=0.22$.

Dimensionless results for G will be presented. They are obtained, following [6, 7], by dividing the values of G by $G_0=\left(1+\kappa^m/8\mu^m\right)\sigma_0^2 a\pi$, where $\kappa^m=3-4\nu^m$, μ^m is the shear modulus of the matrix and σ_0 is the external applied compression. The fibre radius considered is $a=7.5\cdot10^{-6}m$.

3. Failure initiation

The presence of an external secondary load, σ_{33}, acting at the same time as $\sigma_{22} < 0$ could alter the origin of the failure and, thus, the development of the interface crack. The initiation of the failure at the interface has been considered in this work to be controlled by the $\sigma_{r\theta}$ distribution [8], at the undamaged interface, as was already done in [1]. Then, it is fundamental to analyze the influence that the different levels of σ_{33} have on $\sigma_{r\theta}$ of the undamaged interface. Three different values of coefficient n have been considered: 0, 0.5 and 1. Based on this the notation employed to distinguish between the different biaxial cases follows the scheme: C-*n*T and C-*n*C (T=tension, C=compression).

Curves presented in Fig. 3a (C-*n*T casec) show that their shape and the location of the maxima are not altered by the presence of $\sigma_{33} > 0$. However, the $\sigma_{r\theta}$ level becomes higher as n increases. Thus, a possible first debond would still be located at $\alpha = 45º$, $135º$, $225º$ or $315º$, as occurred in the C-0 case, and require a lower value of the external load, σ_0, as n increases.

Referring to the C-*n*C cases, Fig. 3b, it can be observed that although the qualitative evolution of $\sigma_{r\theta}$ seems not to be affected by the increasing presence of $\sigma_{33} < 0$, its level decreases as n increases. In view of this observation it seems feasible that the shear stresses cause damage at the interface whenever coefficient n does not reach its limit value $n = 1$, although the required external load σ_0 needs to be increased as n is. The first debonds would then be located at $\alpha = 45º, 135º$, $225º$ or $315º$.

Based on the former evidence, an initial debond at the interface of 10º length at $\alpha = 135º$ will be assumed for the study of the interface crack, both for the C-*n*C cases and the C-*n*T cases.

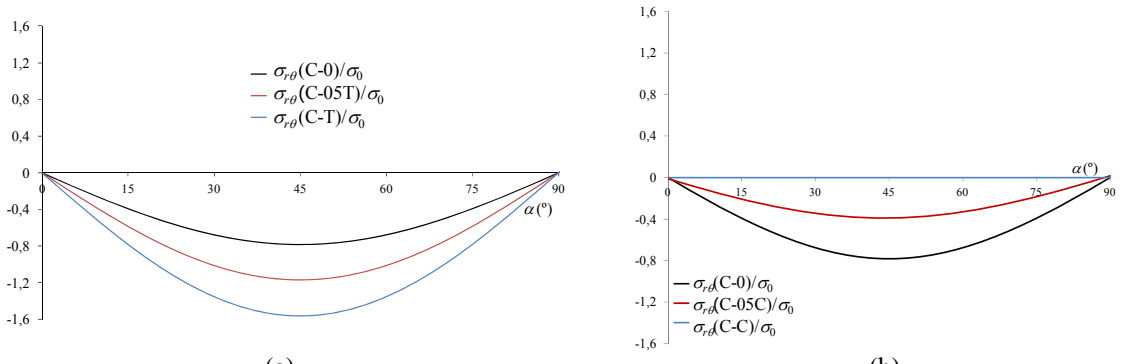

(a) (b)

Figure 3. $\sigma_{r\theta}$ distribution at the undamaged interface for (a) C-*n*T cases and (b) C-*n*C cases.

4. Interface crack

The evolution of the first debond at the interface is studied by means of the BEM model shown in Fig. 2a and its growth evaluated in terms of the Energy Release Rate, G, Eq. (1).

4.1. Compression-tension biaxial case

The evolution of the Energy Release Rate associated to the lower tip of the interface crack has been calculated for three different C-*n*T cases: $n = 0.25, 0.5$ and 1, and compared with the

uniaxial case, C-0, Fig. 4(a). It is necessary to remark the higher level of the obtained G evolution as n increases. This difference is more noticeable for large debonds, almost reaching an order of difference between C-0 and C-T cases for the largest debond considered. This indicates that the propagation of the initial debond would require a lower level of σ_0 as n increases.

The prediction of growth of the interface crack is made by comparing G with its corresponding critical value, G_c [9]. G - G_c comparisons for the cases C-0 and C-0.1T (taken as representative of all C-nT cases) are plotted in Fig. 4(b). A value of 0.25 has been chosen for λ, and G_{1c} has been taken as the value that makes G and G_c coincide for the first debonding angle, $\theta_d = 10^o$ in this case. This criterion for the election of G_{1c} can be applied once a scaled representation of the G curves, that makes them to coincide at $\theta_d = 10^o$, has been implemented.

The results presented in Fig. 4(b) make it possible to predict that the range of unstable growth of the interface crack widens as $\sigma_{33} > 0$ increases, even reaching a significant difference, for high values of n coefficient (not represented in the figure), with respect to the growth at the interface in the case of uniaxial compression. In particular, it can be checked in the Figure that Mode I does not disappear until the lower crack tip reaches a position of $\alpha = 212^o$ (for which a physically relevant contact zone next to the lower crack tip is detected). Taking into account that the difference between the evolutions of G and G_c will be reduced by the presumably presence of friction at the contact zone, whose effect will become more significant as the contact zone increases, it is then possible to predict an unstable growth of the crack tip, at least up to $\alpha = 212^o$.

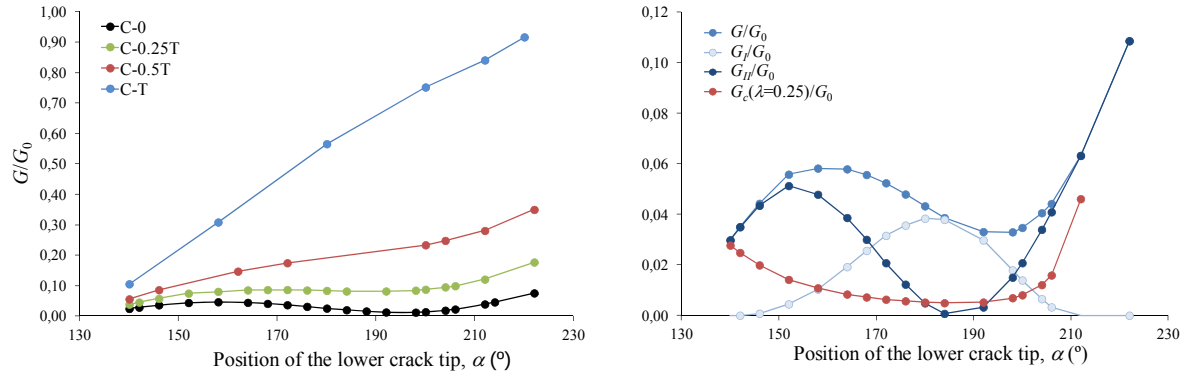

Figure 4. (a) G evolution of the lower interface crack tip (C-nT cases). (b) G_I, G_{II} and G evolutions of the lower interface crack tip (C-0.1T case).

4.2. Compression-compression biaxial case

In order to evaluate the effect of $\sigma_{33} < 0$, G at the lower crack tip is calculated in this section for the C-0.5C case and compared with that obtained for the C-0 case [1], Fig. 5(a). The results lead to the conclusion that it would be necessary to apply a higher external load, σ_0, in the C-0.5C case than in the uniaxial one for the interface crack to propagate. Besides, and although not included in the figure, it can be checked that Mode I contribution is minimal

versus Mode II one for the C-0.5C case. Thus, $\sigma_{33} < 0$ would inhibit the progress of this type of damage.

Fig. 5(b) contains the G evolution of the interface crack for different positions of its lower tip, C-0.5C case, together with its corresponding $G_c(\lambda = 0.2)$. G evolution has been scaled in order to coincide at its initial point with the value of the uniaxial case, as in the C-*n*T cases, so that G_{1c} value is the same for both cases, $n = 0$ and $n = 0.5$.

The $G - G_c$ comparison shown in Fig. 5(b) demonstrates that it would be necessary to apply a higher level of external load, σ_0, for the initial debond to propagate, or, alternatively, the length of the initial debond considered would have to be longer. However, if the propagation of the initial defect started, its range of unstable growth would be lower than in the uniaxial case.

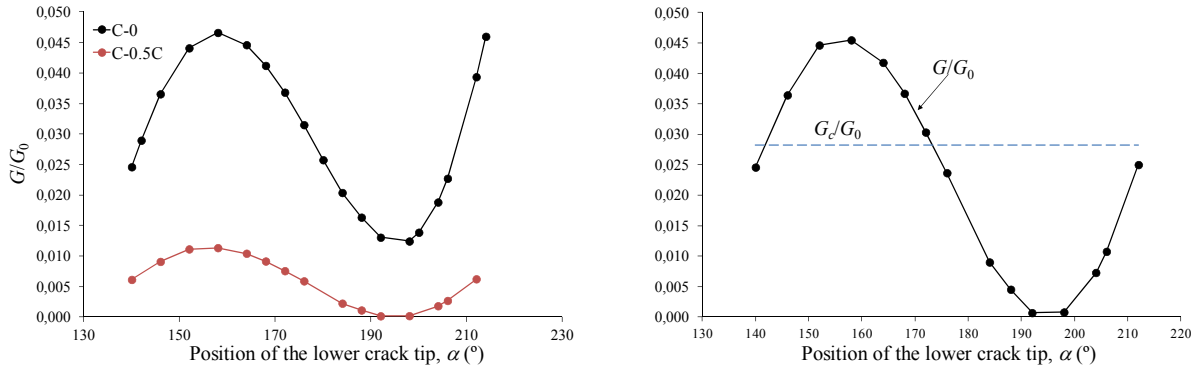

(a) (b)

Figure 5. (a) G evolution at the lower interface crack tip (C-*n*C cases, *n*=0, 0.5) (b) $G - G_c$ comparison (C-0.5C case).

5. Growth through the matrix

The stable position reached by the crack at the interface after a period of unstable propagation warns about the possible occurrence of a different stage in the mechanism of damage under study. Following with the steps already detected for the C-0 case the possibility of kinking towards the matrix is analysed next.

The first step of the kinking analysis consists in the study of the circumferential stress around the interface crack tip in order to identify the preferential direction of kinking, associated to the maximum circumferential stress, $\sigma_{\theta\theta}^{max}$, for each position of the interface crack, according to the Maximum Circumferential Stress Criterion [11]. In addition, an energetic evaluation of the propagation of the crack in the matrix, once kinked, has been carried out.

5.1. Compression-tension biaxial case

The model presented in Fig. 2a has been used for this analysis and the distribution of $\sigma_{\theta\theta}$ has been performed for two positions of the lower tip, $\alpha = 204º$ and $\alpha = 214º$, Figs. 6(a) and (b), respectively, associated to the C-0.1T case. The first one corresponds to a position within the expected range of kinking propagation for the C-0 uniaxial case [2] and the second one is located within the range of ending established for the C-0.1T in Fig. 4(b). Three different

distances, R , to the crack tip [*0.001a*, *0.005a*, *0.01a*] have been considered. The results obtained for $\alpha = 204º$, Fig. 6(a), conclude in a range of preferential orientation of the crack in the matrix, θ, corresponding to $60º \le \theta \le 63º$, and $57º \le \theta \le 60º$ for $\alpha = 214º$.

Once the preferential kinking direction of the interface crack has been calculated it is necessary to study the kinking occurrence from an energetic point of view. To this end the model shown in Fig. 2(b) has been used to consider, at $\alpha = 214º$, the presence of small kinked cracks subjected to a C-0.1T loading state. The orientations of these kinked cracks, given by θ_{kink}, cover the range 45º-60º. The results obtained, Fig. 7, point to Mode I dominancy in the G^m distribution (ERR of the crack in the matrix). It can also be checked that G^m maintains a fairly constant level within the orientation range considered, thus not clearly determining a preferential kinking orientation within the matrix. On the other hand, G^{int} (ERR of the interface crack, also included in the Figure) shows pure Mode II character, as was already detected in Fig. 4(b), and is lower than G^m for all orientations considered.

Finally, based on the relative values of G_c for the interface and the matrix and the different character of growth for both possibilities, favourable conditions are found for the kinking of the interface crack towards the matrix once it has reached a stable position at the interface.

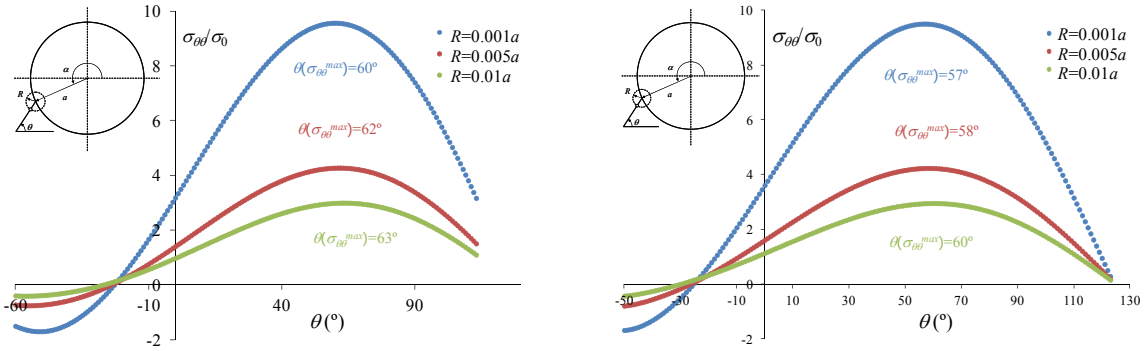

(a) (b)

Figure 6. $\sigma_{\theta\theta}$ distribution around the lower crack tip (a) $\alpha = 204º$ (b) $\alpha = 214º$. C-0.1T case.

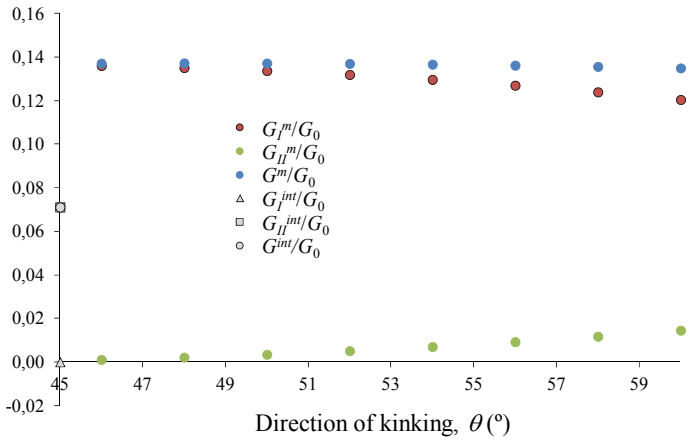

Figure 7. G_I, G_{II} and G of the kinked crack following different orientations. ($\alpha = 214º$).

5.2. Compression-compression biaxial case

The maximum circumferential stress distribution is represented in Fig. 8(a) for a position of the lower crack tip $\alpha = 176º$ (C-0.5C case) and $R = 0.001a, 0.005a$ and $0.01a$. The results show that $\sigma_{\theta\theta}$ takes negative values for all orientations towards the matrix considered, which, based on the criterion employed, would impede the kinking towards the matrix. As a consequence, the crack would be trapped at the interface although showing a limited growth in comparison with the uniaxial case. Thus, the progression of the inter-fibre failure in this case would be inhibited and the appearance of alternative mechanisms of failure not considered in this work might occur.

For the cases with relatively small $\sigma_{33} < 0$, kinking would be possible, and thus, the mechanism of failure established for the C-0 case would prevail. Moreover, if the circumferential stress analysis is repeated for the C-0.1C case, Fig. 8(b), tensions are detected, their maxima being located within the range 49º-65º. It should be pointed out that a noticeable decrease in the circumferential stress level is detected in this case compared with the uniaxial case [2], which would again reduce the possibilities of kinking.

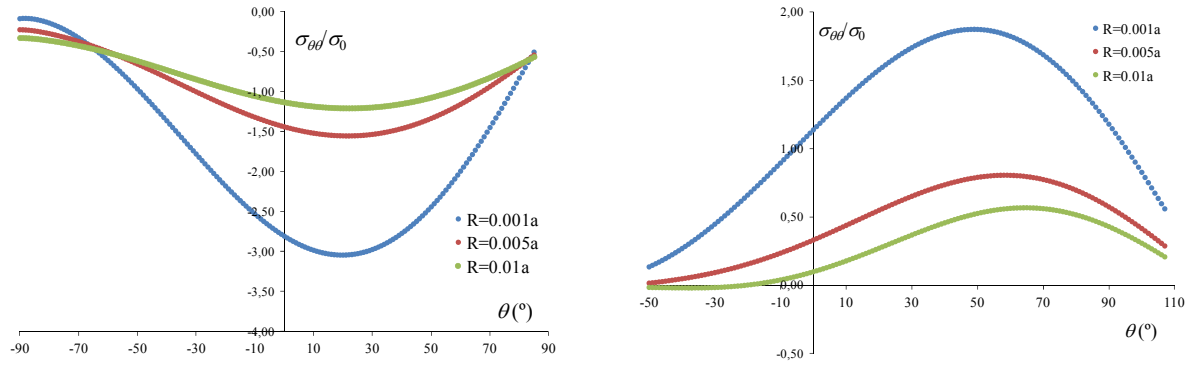

(a) (b)

Figure 8. $\sigma_{\theta\theta}$ distribution around the lower crack tip for $\alpha = 176º$ (a) C-0.5C case, (b) C-0.1C case.

6. Conclusions

The first stages of the development of the compression dominated inter-fibre failure under biaxial loads have been studied by means of single fibre BEM models. A secondary external load has been considered to act simultaneously with the compression nominally responsible for the failure, and both cases (tension and compression) have been analysed.

The results obtained show that the presence of a secondary load could alter several aspects of the stages already detected for the inter-fibre failure under uniaxial compression, leading to the conclusion that the presence of a secondary tension accelerates the generation of failure whereas a secondary compression inhibits it. As a consequence, the presence of an out plane stress component could affect the development of the failure. Additional details of the work can be found in [12].

Acknowledgements

This work was supported by the Spanish Ministry of Education and Science/Economy and Competitiveness and Junta de Andalucía (Projects MAT2012-37387, DPI 2012-37187, TEP-4051 and TEP-7093).

References

[1] E. Correa, V. Mantič and F. París. Numerical characterization of the fibre-matrix interface crack growth under transverse compression. *Eng Fract Mech*, 75(14): 4085-4103, 2008.
[2] E. Correa, V. Mantič and F. París. A micromechanical view of inter-fibre failure of composite materials under compression transverse to the fibres. *Compos Sci Technol*, 68: 2010-2021, 2008.
[3] V. Mantič, A. Blázquez, E. Correa and F. París. F. Analysis of interface cracks with contact in composites by 2D BEM. In Guagliano M., Aliabadi M.H., editors, *Fracture and Damage of Composites*, pages 189-248. WIT Press, Southampton, 2006.
[4] F. París and J. Cañas. *Boundary Element Method. Fundamentals and Applications*. Oxford: OUP; 1997.
[5] G.R. Irwin. Analysis of stresses and strain near the end of a crack transversing a plate. *J App Mech*, 24: 361-364, 1957.
[6] M.A. Toya. A crack along the interface of a circular inclusion embedded in an infinite solid. *J. Mech Phys Solids*, 22: 325-348, 1974.
[7] Y. Murakami. *Stress Intensity Factor Handbook*. Oxford: Pergamon Press, 1988.
[8] J.N. Goodier. Concentration of stress around spherical and cylindrical inclusions and flaws. *App Mech*, 55: 39-44, 1933.
[9] J.W. Hutchinson and Z. Suo. Mixed mode cracking in layered materials. *Adv App Mech*, 29: 63-191, 1992.
[10] V. Mantič and F. París. Relation between SIF and ERR based measures of fracture mode mixity in interface cracks. *Int J Fracture*, 130: 557-569, 2004.
[11] F. Erdogan and G. C. Sih. On the crack extension in plates under plane loading and transverse shear. *J Basic Eng*, 85: 519-527, 1963.
[12] E. Correa, F. París and V. Mantič. Effect of a secondary transverse load on the inter-fibre failure under compression. *Composites Part B*, doi: http://dx.doi.org/10.1016/j.compositesb.2014.01.005, 2014.